IRIS AperTO

UNIVERSITÀ DEGLI STUDI DI TORINO

AperTO - Archivio Istituzionale Open Access dell'Università di Torino

Tumor heterogeneity and Lesion-Specific response to targeted therapy in colorectal cancer

This is the author's manuscript

Original Citation:

Availability:

This version is available http://hdl.handle.net/2318/1573141 since 2016-06-27T18:03:51Z

Published version:

DOI:10.1158/2159-8290.CD-15-1283

Terms of use:

Open Access

Anyone can freely access the full text of works made available as "Open Access". Works made available under a Creative Commons license can be used according to the terms and conditions of said license. Use of all other works requires consent of the right holder (author or publisher) if not exempted from copyright protection by the applicable law.

(Article begins on next page)

17 February 2025

This is the author's final version of the contribution published as:

Russo, Mariangela; Siravegna, Giulia; Blaszkowsky, Lawrence S.; Corti, Giorgio; Crisafulli, Giovanni; Ahronian, Leanne G.; Mussolin, Benedetta; Kwak, Eunice L.; Buscarino, Michela; Lazzari, Luca; Valtorta, Emanuele; Truini, Mauro; Jessop, Nicholas A.; Robinson, Hayley E.; Hong, Theodore S.; Mino-Kenudson, Mari; Di Nicolantonio, Federica; Thabet, Ashraf; Sartore-Bianchi, Andrea; Siena, Salvatore; Iafrate, John; Bardelli, Alberto; ^*; Corcoran, Ryan B.; ^*; ^ joint co-last authorship; *joint corresponding authorship. Tumor heterogeneity and Lesion-Specific response to targeted therapy in colorectal cancer. CANCER DISCOVERY. 6 (2) pp: 147-153. DOI: 10.1158/2159-8290.CD-15-1283

The publisher's version is available at:
http://cancerdiscovery.aacrjournals.org/cgi/doi/10.1158/2159-8290.CD-15-1283

When citing, please refer to the published version.

Link to this full text:
http://hdl.handle.net/2318/1573141

This full text was downloaded from iris - AperTO: https://iris.unito.it/

iris - AperTO

University of Turin's Institutional Research Information System and Open Access Institutional Repository

Tumor heterogeneity and lesion-specific response to targeted therapy in colorectal cancer

Mariangela Russo[1,2,*], Giulia Siravegna[1,2,*], Lawrence S. Blaszkowsky[3,4,*], Giorgio Corti[1], Giovanni Crisafulli[1], Leanne G. Ahronian[3,4], Benedetta Mussolin[1], Eunice L. Kwak[3,4], Michela Buscarino[1], Luca Lazzari[1], Emanuele Valtorta[5], Mauro Truini[5], Nicholas A. Jessop[6], Hayley E. Robinson[6], Theodore S. Hong[3,7], Mari Mino-Kenudson[6], Federica Di Nicolantonio[1,2], Ashraf Thabet[8], Andrea Sartore-Bianchi[5], Salvatore Siena[5], A. John Iafrate[6], Alberto Bardelli[1,2,#], Ryan B. Corcoran[3,4,#]

[1]Candiolo Cancer Institute-FPO, IRCCS, Candiolo, Torino, Italy. [2]Department of Oncology, University of Torino, Torino, Italy. [3]Massachusetts General Hospital Cancer Center, Boston, MA, USA. [4]Department of Medicine, Harvard Medical School, Boston, MA, USA. [5]Niguarda Cancer Center, Ospedale Niguarda Ca' Granda, Milan, Italy. [6]Department of Pathology, Massachusetts General Hospital, Boston, MA, USA. [7]Department of Radiation Oncology, Massachusetts General Hospital, Boston, MA, USA. [8]Department of Radiology, Massachusetts General Hospital, Boston, MA, USA.

* Drs. Russo, Siravegna, and Blaszkowsky contributed equally to this article.

\# To whom correspondence should be addressed:

Dr. Ryan B. Corcoran
Massachusetts General Hospital Cancer Center, 149 13th St., 7th floor
Boston, MA 02129
Phone: 617-726-8599
Fax: 617-724-9648
Email: rbcorcoran@partners.org

Dr. Alberto Bardelli
University of Torino, Department of Oncology, FPO, IRCCS
SP 142, Km 3.95, Candiolo (TO), ZIP 10060, Italy
Phone: +39-011-9922548
Email: alberto.bardelli@untio.it

Running Title

Lesion-specific response to therapy in CRC

Key Words

Tumor heterogeneity, drug resistance, colorectal cancer

Disclosure of Potential Conflicts of interest

R.B.C. is a consultant/advisory board member for Genentech, Merrimack Pharmaceuticals, and Avidity Nanomedicines. A.B. is a consultant/advisory board member of Horizon Discovery, Trovagene, and Biocartis. All other authors do not have conflicts of interest to declare.

ABSTRACT

How genomic heterogeneity associated with acquired resistance to targeted agents affects response to subsequent therapy is unknown. We studied EGFR blockade in colorectal cancer to assess whether tissue and liquid biopsies can be integrated with radiological imaging to monitor the impact of individual oncogenic alterations on lesion-specific responses. Biopsy of a patient's progressing liver metastasis following prolonged response to cetuximab revealed a K57T MEK1 mutation as a novel mechanism of acquired resistance. This lesion regressed upon treatment with panitumumab and the MEK inhibitor trametinib. In ctDNA, mutant MEK1 levels declined with treatment, but a previously unrecognized KRAS Q61H mutation was also identified that increased despite therapy. This same KRAS mutation was later found in a separate non-responding metastasis. In summary, parallel analyses of tumor biopsies and serial ctDNA monitoring show that lesion-specific radiographic responses to subsequent targeted therapies can be driven by distinct resistance mechanisms arising within separate tumor lesions in the same patient.

SIGNIFICANCE

Molecular heterogeneity ensuing from acquired resistance drives lesion-specific responses to subsequent targeted therapies. Analysis of a single-lesion biopsy is inadequate to guide selection of subsequent targeted therapies. ctDNA profiles allow the detection of concomitant resistance mechanisms residing in separate metastases and assessment of the effect of therapies designed to overcome resistance.

INTRODUCTION

Personalized cancer medicine approaches, inhibiting kinases in tumors driven by defined genomic alterations, have demonstrated striking efficacy in many cancer types. However, acquired resistance inevitably develops, limiting the benefit of targeted therapies(1). Acquired resistance mechanisms are typically identified by biopsying a single resistant tumor lesion for molecular analysis. This information is sometimes used to guide subsequent therapy for individual patients. For example, recent trials evaluating therapeutic strategies designed to overcome resistance mechanisms actually require identification of a specific molecular alteration in a post-progression tissue biopsy as a condition for enrollment (NCT02192697, NCT02094261).

However, tumors can display high levels of molecular heterogeneity(2-7). Indeed, exposure to therapy may result in selection of sub-clonal cell populations, capable of growing under drug pressures(8-11). Therefore, a single-lesion biopsy at disease progression may vastly underrepresent the molecular heterogeneity of resistant tumor clones in an individual patient and may fail to detect the existence of distinct but important resistance mechanisms that could impact treatment responses.

The impact of tumor heterogeneity, arising as a result of acquired resistance, on response to subsequent lines of targeted therapy has been hypothesized, but never documented definitively. Here, we show that different metastatic biopsies from the same colorectal cancer (CRC) patient display genetically distinct mechanisms of resistance to EGFR blockade. By assessing multiple biopsies in parallel with circulating tumor DNA (ctDNA) analysis, we demonstrate that distinct resistance mechanisms emerging in different metastases in the same patient can drive lesion-specific responses to the next

line of targeted therapy.

RESULTS

Emergence of a MEK1 K57T mutation upon acquired resistance to cetuximab

The patient's initial clinical course is summarized in Fig. 1A. Following adjuvant chemotherapy for stage IIIC colorectal adenocarcinoma, the patient was found to have a new liver metastasis and tumor recurrence at the site of surgical colonic anastomosis. A simultaneous low anterior resection and partial hepatectomy were performed, but she developed new liver metastases 2 months later.

Molecular analysis of the primary tumor revealed wild-type (WT) *KRAS* and *NRAS* genes. The anti-EGFR antibodies, cetuximab and panitumumab, improve survival in combination with chemotherapy in *RAS* WT CRC(12, 13). The patient responded to palliative chemotherapy with irinotecan and cetuximab for 15 months. The clinical response was attributed to cetuximab, as the patient's disease progressed while receiving irinotecan-containing chemotherapy as the prior line of therapy. Ultimately, her liver metastases progressed, and a core needle biopsy of a progressing segment 8 liver metastasis was obtained. The patient's disease continued to progress despite subsequent treatment with FOLFOX and bevacizumab, followed by regorafenib.

Molecular analysis of the post-progression liver metastasis biopsy was performed to determine the mechanism of acquired resistance to cetuximab and to guide subsequent therapy.

The post-progression liver biopsy and the primary tumor were analyzed with a next-generation sequencing panel covering 1000 genes, (Supplementary Table S1). A targeted sequencing panel (Supplementary Table S2) was also performed on these specimens and on two additional tumor specimens obtained prior to treatment with irinotecan and cetuximab (Fig. 1). A truncating mutation in *TP53* at codon 171 (p.E171*; c.511g>t) was identified in all tumor specimens, suggesting that this mutation arose early in the clonal development of this CRC (Fig. 1, Supplementary Table S3). A lysine-to-threonine substitution at codon 57 (p.K57T; c.170a>c) of MEK1 (encoded by the *MAP2K1* gene) was identified in the post-progression liver lesion, but was not detected in all three tumor specimens obtained prior to cetuximab (Fig. 1, Supplementary Table S3). Mutations in p.K57 in MEK1 were recently implicated in *de novo* resistance to anti-EGFR antibodies in CRC(14, 15), they have not previously been observed in the setting of acquired resistance. No other alterations previously implicated in resistance to anti-EGFR antibodies(6, 8, 9, 16) were identified, although the presence of additional subclonal resistance alterations not detected in our analysis of this tumor biopsy cannot be ruled out. MEK1 signals downstream of EGFR, and mutations at p.K57 in MEK1 occur in lung adenocarcinoma and can activate MEK1 kinase activity(17, 18). Thus, MEK1 mutation could bypass the effect of EGFR inhibition and likely represents a novel mechanism of acquired resistance to cetuximab in this patient.

Role of MEK1 mutation in acquired resistance to cetuximab

Modeling acquired resistance to targeted therapies in cancer cells has proven effective in predicting clinically-relevant resistance mechanisms and in guiding therapeutic strategies to overcome resistance(19, 20). A cetuximab-sensitive *RAS*-WT CRC cell line (HCA46) was treated with cetuximab until resistant clones emerged. These resistant

clones developed a lysine-to-asparagine substitution at codon 57 (p.K57N) of MEK1—the same codon mutated in the patient's post-progression biopsy (Fig. 2A, Supplementary Fig. S1A). These cells exhibited constitutive activation (phosphorylation) of MEK and ERK despite cetuximab treatment (Supplementary Fig. S1B). Exogenous expression of either K57T (identified in the patient) or K57N (identified in the cell line) mutant MEK1, but not wild-type MEK1, in an independent *RAS*-WT CRC cell line, LIM1215, was sufficient to confer resistance to cetuximab or panitumumab (Figure 2B, Supplementary Fig.S1C-D). However, the combination of the MEK inhibitor trametinib with either cetuximab or panitumumab was able to restore sensitivity, confirming that EGFR-dependence is maintained in the setting of acquired resistance, and suggesting a potential therapeutic strategy to overcome resistance to EGFR blockade caused by this mutation (Fig. 2C, Supplementary Fig. S2A-E).

Subsequent targeted therapy and serial ctDNA monitoring

Accordingly, the patient was treated with the combination of panitumumab and trametinib, which have been administered together previously(21). The patient's serum carcinoembryonic antigen CEACAM5 (CEA) levels decreased by ~60% during therapy (Fig. 3A). A repeat computed tomography (CT) scan of the abdomen after 3 months of therapy demonstrated a reduction in the size of the patient's segment 8 liver metastasis, which harbored the MEK1 p.K57T mutation (Fig. 3B), but revealed that some other metastatic lesions had in the meantime progressed.

Peripheral blood for plasma ctDNA analysis was collected prior to initiation of panitumumab and trametinib and throughout treatment. Plasma collected prior to therapy was analyzed using a next-generation sequencing method, which we developed

to interrogate 226 cancer-related genes in ctDNA(15). As expected, this analysis detected the *TP53* p.E171* and *MAP2K1* p.K57T variants, but surprisingly unveiled a previously unrecognized *KRAS* p.Q61H (c.183a>c) mutation (Supplementary Table S4). Indeed the *KRAS* p.Q61H mutation was not observed in the segment 8 liver metastasis biopsy by NGS or by high-sensitivity digital droplet polymerase chain reaction (ddPCR) (Fig. 3B, Supplementary Table S3), suggesting that this mutation was not present in this metastasis, but was already present in a separate metastatic lesion at the start of panitumumab and trametinib therapy.

Changes in the relative abundance of specific mutations in ctDNA during panitumumab and trametinib treatment were monitored by ddPCR. Levels of the *TP53* p.E171* variant dropped after initiation of therapy, but rose later during treatment in concert with the patient's CEA levels (Fig. 3A, Supplementary Table S5). Since *TP53* p.E171* was detected in all tumor specimens from this patient, it likely represents an early clonal or "founder" mutation present in all tumor cells, and thus a marker of overall disease burden. Another "founder" mutation, *IGF1R* p.R366W (c.1096c>t), showed a similar pattern (Supplementary Figure S3A-B, Supplementary Tables S5-S6).

However, levels of *MAP2K1* p.K57T declined sharply and remained low throughout treatment, indicating effective suppression of MEK1 mutant clones by panitumumab and trametinib. Suppression persisted even as the patient's CEA and *TP53* p.E171* levels began to rise, suggesting that a different molecular alteration must be driving disease progression (Fig. 3A, Supplementary Table S6). Conversely, *KRAS* p.Q61H rose markedly during therapy, indicating outgrowth of a resistant *KRAS*-mutant clone. Biopsy of a different segment 5 liver metastasis that progressed despite panitumumab and trametinib revealed that this lesion harbored the same *KRAS* p.Q61H mutation identified

in ctDNA, along with the *TP53* p.E171* mutation, but the *MAP2K1* p.K57T mutation was not detected by sequencing or ddPCR (Fig. 3B-C, Supplementary Table S3). Notably, the *KRAS* or *MAP2K1* mutations could not be detected by high-sensitivity ddPCR in any of the tumor specimens obtained prior to the prolonged response to cetuximab (Supplementary Table S3), but preexistence of rare clones harboring these mutations below the limit of detection cannot be excluded.

After 4 months of panitumumab and trametinib, the patient discontinued therapy as CEA levels continued to rise. Analysis of ctDNA obtained one week later revealed a rebound in *MAP2K1* p.K57T levels (Fig. 3A).

DISCUSSION

The inevitable emergence of acquired resistance is a major limitation to the efficacy of targeted therapies in oncology. Identification of actionable resistance mechanisms may offer patients the opportunity to benefit from therapies designed to overcome resistance.

Here, we describe how distinct acquired resistance mechanisms can arise concomitantly in separate metastases within the same patient, leading to mixed responses to subsequent targeted therapies. This demonstrates how molecular analysis of a single-lesion biopsy, currently the diagnostic standard for targeted therapy trials, can regularly fail to detect clinically-relevant molecular alterations, which can be responsible for lesion-specific or even sub-clone-specific clinical response and consequent treatment failure.

In this CRC patient, we identified a MEK1 p.K57T mutation in a biopsy of a single

progressing liver metastasis, following prolonged response to cetuximab. Based on preclinical modeling and characterization of this novel resistance mechanism, the patient was treated with the combination of panitumumab and trametinib. Imaging revealed that the lesion harboring the MEK1 mutation responded. However, a neighboring metastasis progressed and was found to harbor a completely distinct resistance mechanism (*KRAS* p.Q61H), confirming that separate metastases can independently evolve different resistance mechanisms, resulting in striking differences in lesion-specific response to targeted therapy.

Our original single-lesion biopsy was not sufficient to capture the molecular heterogeneity of this patient's cancer and failed to detect the simultaneous presence of an additional resistance mechanism (*KRAS* mutation) that eventually led to treatment failure. This underscores the potential pitfalls of selecting a targeted therapy strategy based on the molecular profile of a single resistant lesion. However, both mutations were readily detectable in ctDNA from blood collected prior to combinatorial therapy.

These findings also illustrate the potential of "liquid biopsies". Not only did real-time ctDNA analysis enable identification of a second resistance mechanism not captured by the single-lesion biopsy, but it did so while the patient still appeared to be responding to therapy, thereby predicting both the timing and cause of impending treatment failure. ctDNA analysis also allowed monitoring of dynamic shifts in the clonal composition of the patient's tumor cells, demonstrating effective on-target suppression of the MEK1 mutant population by panitumumab and trametinib, contrasted with marked expansion of the KRAS mutant population driving disease progression.

In summary, while it has been proposed that tumor heterogeneity developing in the context of acquired resistance may have the potential to impact response to subsequent therapies, this has yet to be clearly documented. Here, we demonstrate how individual metastatic lesions can develop distinct resistance mechanisms to targeted agents, resulting in lesion-specific differences in response to the next line of targeted therapy. As more trials evaluating targeted therapy strategies designed to overcome specific acquired resistance mechanisms enter the clinic, genomic results from single-tumor biopsies should be interpreted with caution. By contrast, liquid biopsy approaches have the potential to detect the presence of simultaneous resistance mechanisms residing in separate metastases in a single patient and to monitor the effects of subsequent targeted therapies. Therefore, ctDNA profiles, serial tumor biopsies and lesion-specific radiographic responses can be integrated to define mechanisms of drug resistance and to guide selection of therapeutic strategies in oncology.

METHODS

Patient care and specimen collection

All biopsies, tumor specimens, and peripheral blood draws for plasma isolation were collected in accordance with Institutional Review Board-approved protocols, to which patients provided written informed consent, and all studies were conducted in accordance with the Declaration of Helsinki. Targeted exome sequencing on clinical tissue specimens using a Clinical Laboratory Improvement Amendment (CLIA)-certified clinical next-generation sequencing assay was performed in the Department of Molecular Pathology at the Massachusetts General Hospital. The patient was treated with panitumumab and trametinib, both approved by the United States Food and Drug Administration, off-label with informed consent, and the patient's insurance company

covered the cost of this therapy. Imaging studies, including computed tomography (CT) and Magnetic Resonance Imaging (MRI) scans were obtained as part of routine clinical care.

Cell lines

HCA46 CRC cells were obtained from ECACC cell line bank. The LIM1215 parental cell line has been described previously(22) and was a kind gift of Prof. Robert Whitehead, Vanderbilt University, Nashville, with permission from the Ludwig Institute for Cancer Research, Zurich, Switzerland. The genetic identity of cell lines were last authenticated no less than three months before performing experiments by Cell ID™ System and by Gene Print® 10 System (Promega), through Short Tandem Repeats (STR) at 10 different loci (D5S818, D13S317, D7S820, D16S539, D21S11, vWA, TH01, TPOX, CSF1PO and amelogenin). Amplicons from multiplex PCR reactions were separated by capillary electrophoresis (3730 DNA Analyzer, Applied Biosystems) and analyzed using GeneMapperID software from Life Technologies. All cell lines were tested and resulted negative for mycoplasma contamination with Venor GeM Classic Kit (Minerva Biolabs).

Plasma Sample Collection

At least 10 mL of whole blood were collected by blood draw using EDTA as anticoagulant. Plasma was separated within 5 hours through 2 different centrifugation steps (the first at room temperature for 10 minutes at 1,600 × g and the second at 3,000 × g for the same time and temperature), obtaining up to 3 mL of plasma. Plasma was stored at -80°C until ctDNA extraction.

ctDNA isolation, genome equivalents quantification (GE/ml plasma), and analysis

ctDNA was extracted from plasma using the QIAamp Circulating Nucleic Acid Kit (QIAGEN) according to the manufacturer's instructions. 6 µl of ctDNA were used as template for each reaction. All samples were analyzed in triplicate. PCR reactions were performed using 10 µl final volume containing 5 µl GoTaq® qPCR Master Mix, 2X with CXR Reference Dye) (Promega) and LINE-1 [12,5 µmol] forward and reverse primers. DNA at known concentrations was also used to build the standard curve. Primer sequences are available upon request. Analysis of ctDNA by NGS and ddPCR was performed as previously described(15). Detailed methods are provided in the *Supplementary Methods*.

Cell culture and generation of resistant cells

HCA46 cells were cultured in DMEM medium (Invitrogen), supplemented with 10% FBS, 2mM L-glutamine, antibiotics (100U/mL penicillin and 100 mg/mL streptomycin) and grown in a 37°C and 5% CO2 air incubator. LIM1215 were cultured in RPMI medium (Invitrogen), supplemented with 1µg/ml insulin.

HCA46 cetuximab-resistant derivatives were obtained by exposing cells to a chronic dose of 100µg/ml of cetuximab until resistant derivatives emerged.

Mutational analysis in cell lines

Genomic DNA samples were extracted by Wizard® SV Genomic DNA Purification System (Promega). For Sanger Sequencing, all samples were subjected to automated sequencing by ABI PRISM 3730 (Applied Biosystems). Primer sequences for *MAP2K1* (exon2) are listed elsewhere(17, 19).

Ectopic expression of MEK1 in CRC cells.

LIM1215 RAS wild-type cetuximab-sensitive cells were cultured in RPMI medium (Invitrogen) supplemented with 10% FBS, 1μg/ml insulin, 2mM L-glutamine, antibiotics (100U/mL penicillin and 100 mg/mL streptomycin) and grown in a 37°C and 5% CO2 air incubator. LIM1215 were transduced with lentiviral vector encoding MEK1 WT, MEK1 K57N or MEK1 K57T cDNA. MEK overexpression was verified by western blot analysis.

Drug proliferation assay

CRC cell lines were seeded at different densities (2-3 x10^3 cells/well) in 100μl complete growth medium in 96-well plastic culture plates at day 0. The following day, serial dilutions of the indicated drugs were added to the cells in serum-free medium, while medium-only (in case of cetuximab and panitumumab) or DMSO-only (in case of trametinib) treated cells were included as controls. Plates were incubated at 37°C in 5% CO2 for 4 or 5 days, after which cell viability was assessed by measuring ATP content through Cell Titer-Glo® Luminescent Cell Viability assay (Promega). Luminescence was measured by Perkin Elmer Victor X4.

Western blotting analysis

Prior to biochemical analysis, all cells were grown in their specific media supplemented with 10% FBS with or without indicated drug treatment. Total cellular proteins were extracted by solubilizing the cells in EB buffer (50 mM Hepes pH 7.4, 150 mM NaCl, 1% Triton X-100, 10% glycerol, 5mM EDTA, 2mM EGTA; all reagents were from Sigma-Aldrich, except for Triton X-100 from Fluka) in the presence of 1 mM sodium orthovanadate, 100 mM sodium fluoride and a mixture of protease inhibitors. Extracts were clarified by centrifugation, normalized with the BCA Protein Assay Reagent kit (Thermo). Western blot detection was performed with enhanced chemiluminescence system (GE Healthcare) and peroxidase conjugated secondary antibodies (Amersham).

The following primary antibodies were used for western blotting (all from Cell Signaling Technology, except where indicated): anti-phospho-p44/42 ERK (Thr202/Tyr204); anti-p44/42 ERK; anti-phospho-MEK1/2 (Ser217/221), anti-MEK1/2; anti-phospho AKT (T308); anti-AKT; anti-vinculin (Millipore).

GRANT SUPPORT

This study was supported by grants from the NIH/NCI Gastrointestinal Cancer SPORE P50 CA127003, a Damon Runyon Clinical Investigator Award, and NIH/NCI 1K08CA166510 (all to R.B.C.); and by European Community's Seventh Framework Programme under grant agreement no. 602901 MErCuRIC (A.B.); IMI contract n. 115749 CANCER-ID (A.B.); AIRC 2010 Special Program Molecular Clinical Oncology 5 per mille, Project n. 9970 (A.B.); AIRC IG n. 12812 (A.B.); Fondazione Piemontese per la Ricerca sul Cancro-ONLUS 5 per mille 2010 e 2011 Ministero della Salute (A.B.); Ministero dell'Istruzione, dell'Università e della Ricerca - progetto PRIN 2010-2011 (A.B.)

REFERENCES

1. Garraway LA, Janne PA. Circumventing cancer drug resistance in the era of personalized medicine. Cancer discovery. 2012;2:214-26.

2. Gerlinger M, Horswell S, Larkin J, Rowan AJ, Salm MP, Varela I, et al. Genomic architecture and evolution of clear cell renal cell carcinomas defined by multiregion sequencing. Nat Genet. 2014;46:225-33.

3. Vogelstein B, Papadopoulos N, Velculescu VE, Zhou S, Diaz LA, Kinzler KW. Cancer genome landscapes. Science. 2013;339:1546-58.

4. McGranahan N, Swanton C. Biological and Therapeutic Impact of Intratumor Heterogeneity in Cancer Evolution. Cancer Cell. 2015;27:15-26.

5. Gerlinger M, Rowan AJ, Horswell S, Larkin J, Endesfelder D, Gronroos E, et al. Intratumor heterogeneity and branched evolution revealed by multiregion sequencing. The New England journal of medicine. 2012;366:883-92.

6. Bettegowda C, Sausen M, Leary RJ, Kinde I, Wang Y, Agrawal N, et al. Detection of circulating tumor DNA in early- and late-stage human malignancies. Sci Transl Med. 2014;6:224ra24.

7. Piotrowska Z, Niederst MJ, Karlovich CA, Wakelee HA, Neal JW, Mino-Kenudson M, et al. Heterogeneity Underlies the Emergence of EGFRT790 Wild-Type Clones Following Treatment of T790M-Positive Cancers with a Third-Generation EGFR Inhibitor. Cancer Discov. 2015;5:713-22.

8. Diaz LA, Jr., Williams RT, Wu J, Kinde I, Hecht JR, Berlin J, et al. The molecular evolution of acquired resistance to targeted EGFR blockade in colorectal cancers. Nature. 2012;486:537-40.

9. Misale S, Yaeger R, Hobor S, Scala E, Janakiraman M, Liska D, et al. Emergence of KRAS mutations and acquired resistance to anti-EGFR therapy in colorectal cancer. Nature. 2012;486:532-6.

10. Ahronian LG, Sennott EM, Van Allen EM, Wagle N, Kwak EL, Faris JE, et al. Clinical Acquired Resistance to RAF Inhibitor Combinations in BRAF-Mutant Colorectal Cancer through MAPK Pathway Alterations. Cancer discovery. 2015;5:358-67.

11. Pao W, Miller VA, Politi KA, Riely GJ, Somwar R, Zakowski MF, et al. Acquired resistance of lung adenocarcinomas to gefitinib or erlotinib is associated with a second mutation in the EGFR kinase domain. PLoS Med. 2005;2:e73.

12. Van Cutsem E, Kohne CH, Hitre E, Zaluski J, Chang Chien CR, Makhson A, et al. Cetuximab and chemotherapy as initial treatment for metastatic colorectal cancer. The New England journal of medicine. 2009;360:1408-17.

13. Douillard JY, Oliner KS, Siena S, Tabernero J, Burkes R, Barugel M, et al. Panitumumab-FOLFOX4 treatment and RAS mutations in colorectal cancer. The New England journal of medicine. 2013;369:1023-34.

14. Bertotti A, Papp E, Jones S, Adleff V, Anagnostou V, Lupo B, et al. The genomic landscape of response to EGFR blockade in colorectal cancer. Nature. 2015;526:263-7.

15. Siravegna G, Mussolin B, Buscarino M, Corti G, Cassingena A, Crisafulli G, et al. Clonal evolution and resistance to EGFR blockade in the blood of colorectal cancer patients. Nature medicine. 2015;21:795-801.

16. Arena S, Bellosillo B, Siravegna G, Martinez A, Canadas I, Lazzari L, et al. Emergence of Multiple EGFR Extracellular Mutations during Cetuximab Treatment in Colorectal Cancer. Clinical cancer research : an official journal of the American Association for Cancer Research. 2015;21:2157-66.

17. Marks JL, Gong Y, Chitale D, Golas B, McLellan MD, Kasai Y, et al. Novel MEK1 mutation identified by mutational analysis of epidermal growth factor receptor signaling pathway genes in lung adenocarcinoma. Cancer Res. 2008;68:5524-8.

18. Arcila ME, Drilon A, Sylvester BE, Lovly CM, Borsu L, Reva B, et al. MAP2K1 (MEK1) Mutations Define a Distinct Subset of Lung Adenocarcinoma Associated with

Smoking. Clinical cancer research : an official journal of the American Association for Cancer Research. 2015;21:1935-43.

19. Misale S, Arena S, Lamba S, Siravegna G, Lallo A, Hobor S, et al. Blockade of EGFR and MEK intercepts heterogeneous mechanisms of acquired resistance to anti-EGFR therapies in colorectal cancer. Science translational medicine. 2014;6:224ra26.

20. Prahallad A, Sun C, Huang S, Di Nicolantonio F, Salazar R, Zecchin D, et al. Unresponsiveness of colon cancer to BRAF(V600E) inhibition through feedback activation of EGFR. Nature. 2012;483:100-3.

21. Van Cutsem E, Atreya C, André T, Bendell J, Schellens J, Gordon M, et al. LBA-07Updated Results of the MEK inhibitor trametinib (T), BRAF inhibitor dabrafenib (D), and anti-EGFR antibody panitumumab (P) in patients (pts) with BRAF V600E mutated (BRAFm) metastatic colorectal cancer (mCRC). Annals of Oncology. 2015;26:iv119.

22. Whitehead RH, Macrae FA, St John DJ, Ma J. A colon cancer cell line (LIM1215) derived from a patient with inherited nonpolyposis colorectal cancer. J Natl Cancer I. 1985;74:759-65.

FIGURE LEGENDS

Figure 1: Initial treatment course and analysis of serial tumor biopsies.

The initial clinical course of the CRC patient is summarized, with serum carcinoembryonic antigen (CEA, normal defined as <3.5 ng/mL) tumor marker levels shown throughout treatment. Shaded areas indicate periods of administration of the indicated chemotherapeutic agents: 5-fluorouracil (5FU), oxaliplatin (OX), irinotecan (IRI), cetuximab (CET), radiation therapy (XRT), bevacizumab (BEV), regorafenib (REG). Arrows indicate timing of tumor specimen acquisition from surgical procedures or biopsy. At the bottom of panel A, sequencing data for each specimen are summarized. A p.K57T missense mutation in the *MAP2K1* gene (which encodes for MEK1 protein) was detected in a progressing liver lesion following a prolonged response to cetuximab and irinotecan. The *MAP2K1* p.K57T mutation was not detected in tumor specimens gathered prior to cetuximab and irinotecan therapy (specimens 1-3). Conversely, a nonsense mutation in *TP53* at codon 171 (p.E171*) was detectable in all tumor specimens throughout the clinical course. Variant reads as a fraction of total sequencing reads are shown, with the variant allele percentage shown in parentheses.

Figure 2: MEK1 K57 mutations confer resistance to anti-EGFR therapies.

(A-C) Cetuximab-resistant preclinical models were derived *in vitro* from HCA46, a *RAS*-wildtype CRC cell line. (A) The sensitivity of parental cells and resistant clones to cetuximab and panitumumab in an *in vitro* viability assay are shown. (B) Exogenous expression of MEK1 K57T or MEK1 K57N in an independent cetuximab-sensitive *RAS*-WT CRC cell line (LIM1215) confers resistance to cetuximab, relative to expression of WT MEK1. (C) The combination of 50μg/ml cetuximab (Cetux) and 2nM trametinib (Tramet) or 50μg/ml panitumumab (Panit) and 2nM trametinib can restore sensitivity to

MEK1 mutated cetuximab-resistant clones.

Figure 3. Serial analysis of plasma circulating tumor DNA during subsequent therapy with panitumumab and trametinib.

(A) Timing of panitumumab and trametinib administration is denoted by the grey bar. Timing of discontinuation of therapy is indicated by the dashed line. Serum CEA levels were monitored throughout treatment. Serial assessments of plasma circulating tumor DNA for the percent abundance of variant alleles for *TP53* p.E171* (an early mutational event, present in all of the patient's tumor cells), *MAP2K1* (MEK1) p.K57T, and *KRAS* p.Q61H are shown throughout treatment. While levels of the known *MAP2K1* p.K57T mutation decreased during therapy with panitumumab and trametinib, a *KRAS* p.Q61H mutation was discovered in the plasma, which increased steadily throughout treatment. (B) Axial CT images of the abdomen taken at the start of panitumumab and trametinib therapy (July 2014) and after approximately three months of therapy (November 2014) show a decrease in the size of the segment 8 liver lesion, which harbored the MEK1 K57T mutation. Sequencing data from the biopsy of this lesion obtained after progression on cetuximab and irinotecan and prior to panitumumab and trametinib therapy is summarized on the right. Variant reads as a fraction of total reads are shown, with the variant allele percentage shown in parentheses. (C) Conversely, CT images show that a segment 5 liver lesion increased in size despite therapy with panitumumab and trametinib over the same time period. The segment 5 liver lesion was biopsied after progression on panitumumab and trametinib, and next-generation sequencing detected the same *KRAS* p.Q61H mutation that was identified in the plasma ctDNA, as well as the *TP53* p.E171* mutation present in all tumor specimens from this patient, as summarized on the right. The *MAP2K1* p.K57T mutation that was present in the segment 8 liver lesion was not detected in this biopsy of the segment 5 liver lesion, suggesting

independent evolution of distinct resistance mechanisms in these two metastatic lesions.

Russo et al, Fig. 1

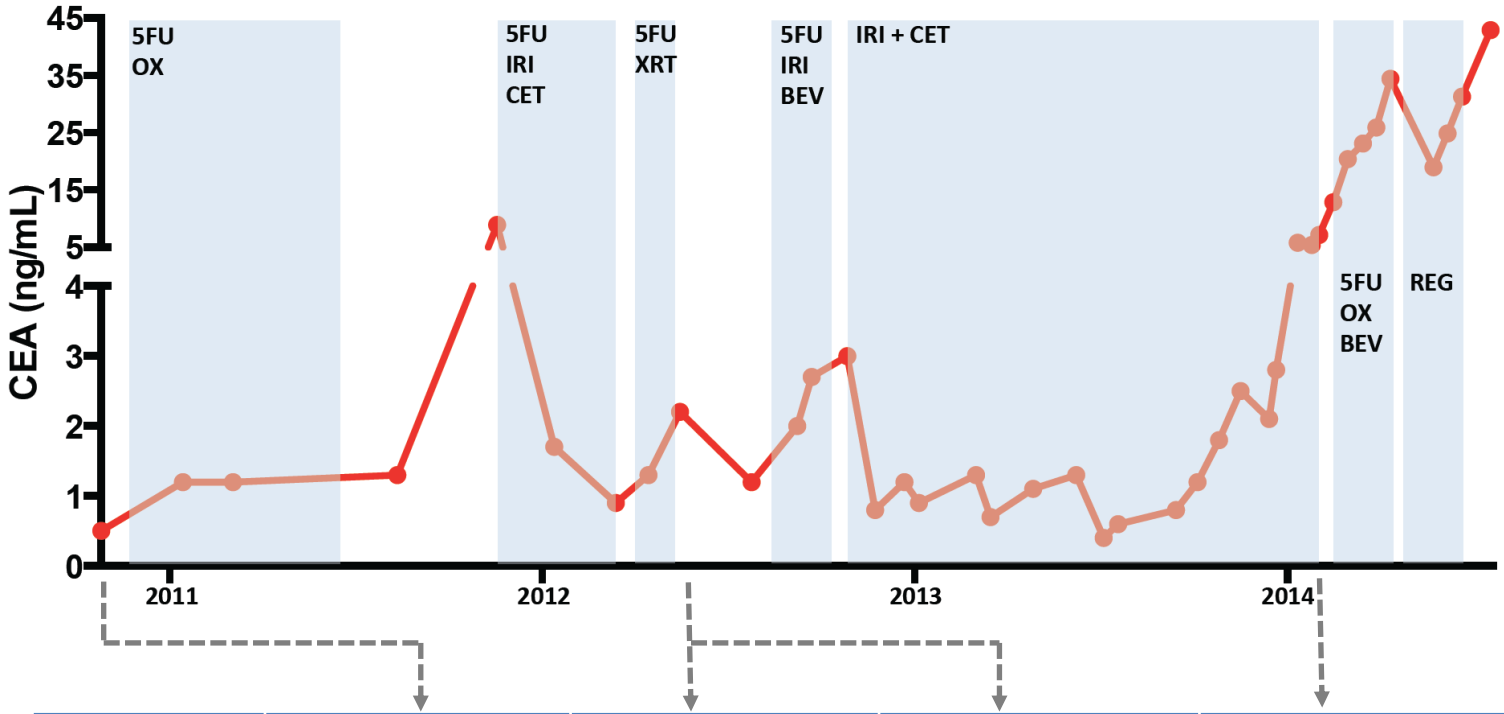

variant	1.) Left colectomy	2.) Low anterior resection	3.) Partial hepatectomy	4.) Post-progression biopsy (liver lesion)
TP53 p.E171*	124/363 (34.2%)	5/93 (5.4%)	167/322 (51.9%)	299/474 (63.1%)
MAP2K1 (MEK1) p.K57T	0/93 (0%)	0/89 (0%)	0/416 (0%)	35/309 (11.3%)

Russo et al, Fig. 2

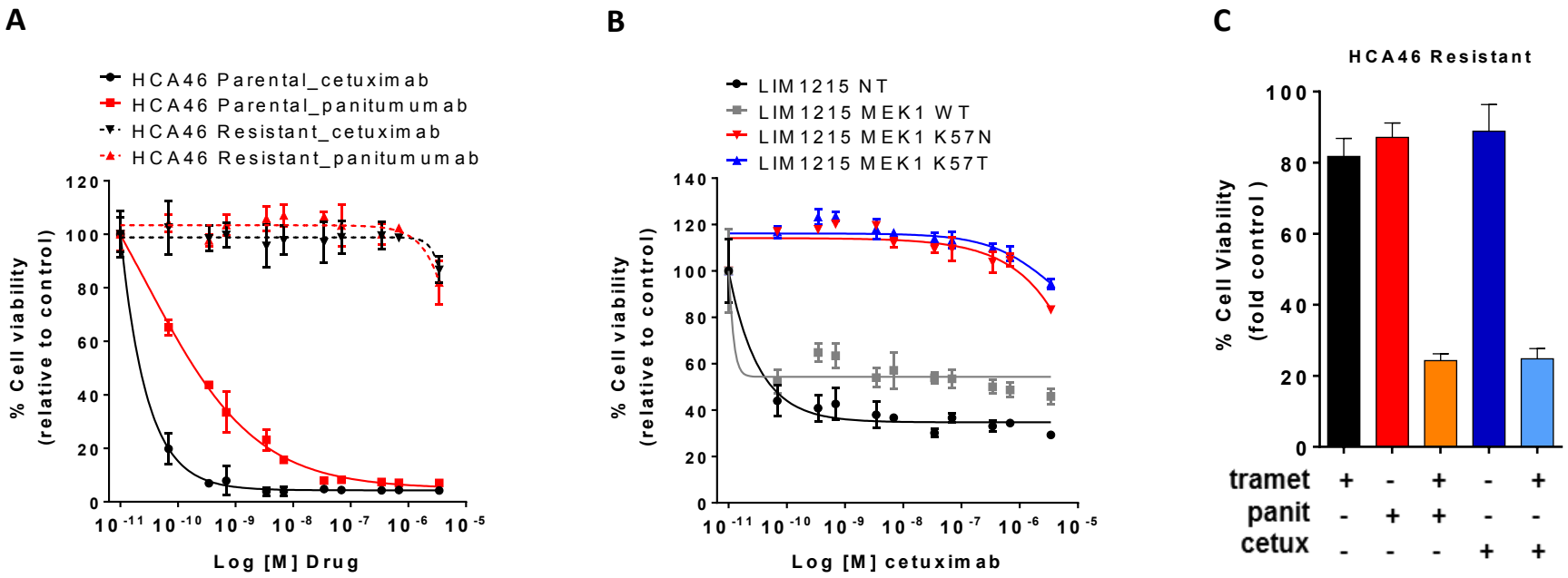

Russo et al, Fig. 3

A

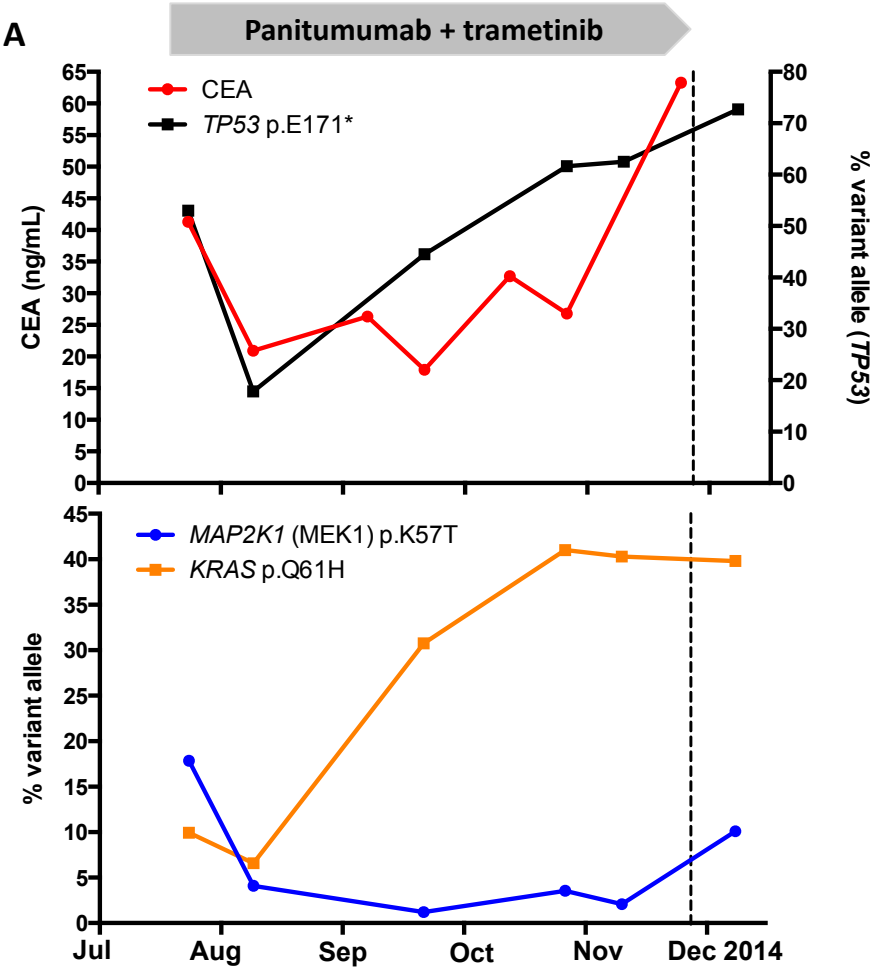

B

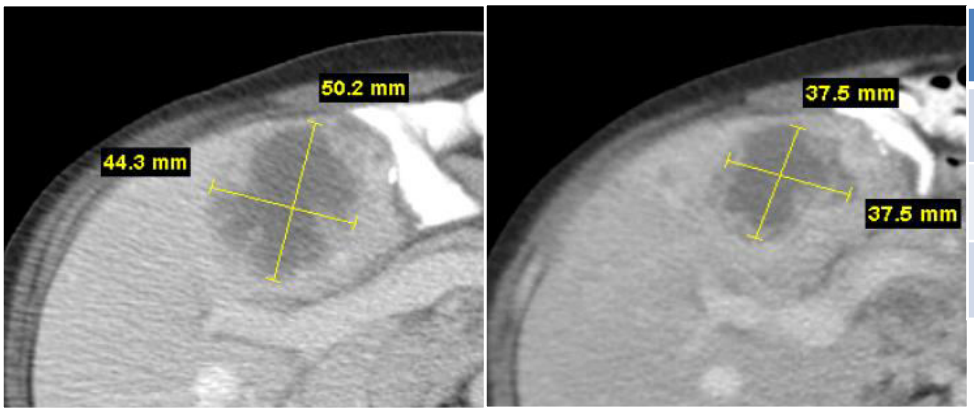

variant	variant allele percentage
TP53 p.E171*	299/474 (63.1%)
***MAP2K1* (MEK1) p.K57T**	**35/309 (11.3%)**
KRAS p.Q61H	0/256 (0%)

C

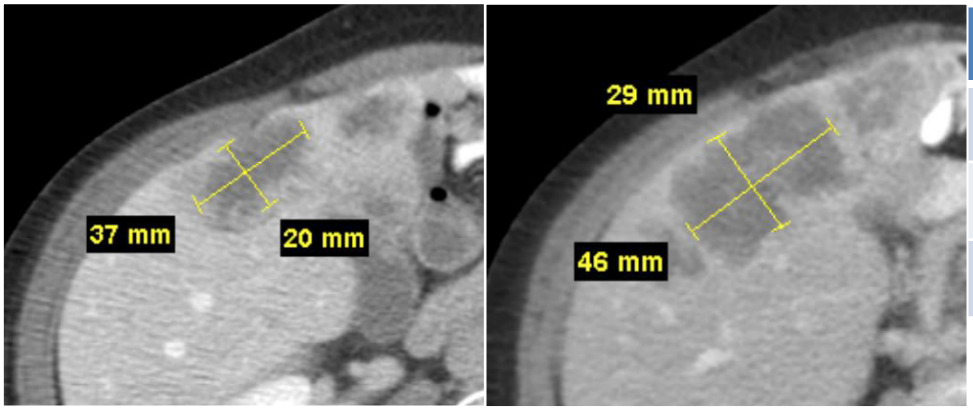

variant	variant allele percentage
TP53 p.E171*	151/387 (39.0%)
MAP2K1 (MEK1) p.K57T	0/186 (0%)
***KRAS* p.Q61H**	**92/302 (30.5%)**

Supplementary Material for

Tumor heterogeneity and lesion-specific response to targeted therapy in colorectal cancer

Mariangela Russo*, Giulia Siravegna*, Lawrence S. Blaszkowsky*, Giorgio Corti, Giovanni Crisafulli, Leanne G. Ahronian, Benedetta Mussolin, Eunice L. Kwak, Michela Buscarino, Luca Lazzari, Emanuele Valtorta, Mauro Truini, Nicholas A. Jessop, Hayley E. Robinson, Theodore S. Hong, Mari Mino-Kenudson, Federica Di Nicolantonio, Ashraf Thabet, Andrea Sartore Bianchi, Salvatore Siena, A. John Iafrate, Alberto Bardelli#, Ryan B. Corcoran#

Supplementary Methods

Supplementary Figures

- Supplementary Figure S1: MEK1 K57 mutation confers resistance to anti-EGFR antibodies in CRC preclinical models.
- Supplementary Figure S2: Dual blockade of EGFR and MEK restores sensitivity to CRC cells expressing MEK1 K57N or K57T.
- Supplementary Figure S3: Longitudinal analysis of founder mutations in patient plasma during panitumumab and trametinib treatment.

Supplementary Tables

- Supplementary Table S1: 1000 gene sequencing panel.
- Supplementary Table S2: 40 gene targeted sequencing panel.
- Supplementary Table S3: Summary of targeted sequencing and ddPCR data on tissue specimens.
- Supplementary Table S4: Next generation sequencing data from plasma ctDNA.
- Supplementary Table S5: Summary of serial ctDNA analyses.
- Supplementary Table S6: Ratio of resistance-associated genetic alterations and founder mutations in serial plasma ctDNA timepoints.

Supplementary Methods

Next Generation Sequencing analysis

Libraries were prepared with Nextera Rapid Capture Custom Enrichment Kit (Illumina Inc., San Diego, CA, USA), according to the manufacturer's protocol. Preparation of libraries was performed starting from 105 ng of plasma ctDNA and 100 ng of gDNA from PBMC (as corresponding normal reference). gDNA was fragmented using transposones, adding simultaneously adapter sequences. For ctDNA libraries preparation was used NEBNext® Ultra™ DNA Library Prep Kit for Illumina® (New England BioLabs Inc., Ipswich MA). Purified gDNA and ctDNA after tagmentation step were used as template for subsequent PCR to introduce unique sample barcodes. Fragments' size distribution of the DNA was assessed using the 2100 Bioanalyzer with a High Sensitivity DNA assay kit (Agilent Technologies, Santa Clara, CA). Equal amount of DNA libraries were pooled and subjected to targeted panel hybridization capture. Libraries were then sequenced using Illumina MiSeq or NextSeq500 sequencer (Illumina Inc., San Diego, CA, USA).

Droplet digital PCR

8 to 10 µl of DNA template was added to 10 µl of ddPCR™ Supermix for Probes (Bio-Rad) and 2 µl of the primer/probe mixture. This reaction mix was added to a DG8 cartridge together with 60µl of Droplet Generation Oil for Probes (Bio-Rad) and used for droplet generation. Droplets were then transferred to a 96 well plate (Eppendorf) and then thermal cycled with the following conditions: 5 minutes at 95°C, 40 cycles of 94°C for 30s, 55°C for 1 minute followed by 98°C for 10 minutes (Ramp Rate 2°C/sec). Droplets were analyzed with the QX200™ Droplet Reader (Bio-Rad) for fluorescent measurement of FAM and HEX probes. Gating was performed based on positive and negative controls, and mutant populations were identified. The ddPCR data were

analyzed with QuantaSoft analysis software (Bio-Rad) to obtain Fractional Abundance of the mutant DNA alleles in the wild-type/normal background. The quantification of the target molecule was presented as number of total copies (mutant plus WT) per sample in each reaction. Fractional Abundance is calculated as follows: F.A. % = (Nmut/(Nmut+Nwt))*100), where Nmut is number of mutant events and Nwt is number of WT events per reaction. ddPCR analysis of normal control plasma DNA (from cell lines) and no DNA template controls were always included. Samples with too low positive events were repeated at least twice in independent experiments to validate the obtained results.

Bioinformatic analysis

Sequence files were mapped to the hg19 reference genome using BWA-mem algorithm(1); PCR duplicates were then removed and the resulting BAM file(2) was used as input for several pipelines. All analyzes are comparison between a normal and tumor sample. We used a custom script in order to call somatic variations and gene copy-number alterations; Pindel(3) software was instead run in searching for INDEL events. Each result was further annotated by main biological information and COSMIC database occurrence.

Bliss interaction index analysis

Bliss interaction index - defined as the difference between the Observed combined fractional inhibition effect YObs and the Expected combined inhibition YExp (whereby Yexp= InhMEKi + InhEGFRi – InhMEKi *InhEGFRi) – was calculated for each drug combination over a concentration range of trametinib tested with a fixed clinically-relevant dose of EGFR monoclonal antibodies. Yobs> Yexp, Yobs≈Yexp, or Yobs<Yexp, indicate synergistic, independent or antagonistic interaction respectively.

As a consequence, the difference Δ between Yobs and Yexp can indicate synergism, additivity or antagonism when ΔYobs -Yexp (Interaction index) >0, ≈0 or <0, respectively.

Supplementary Figures

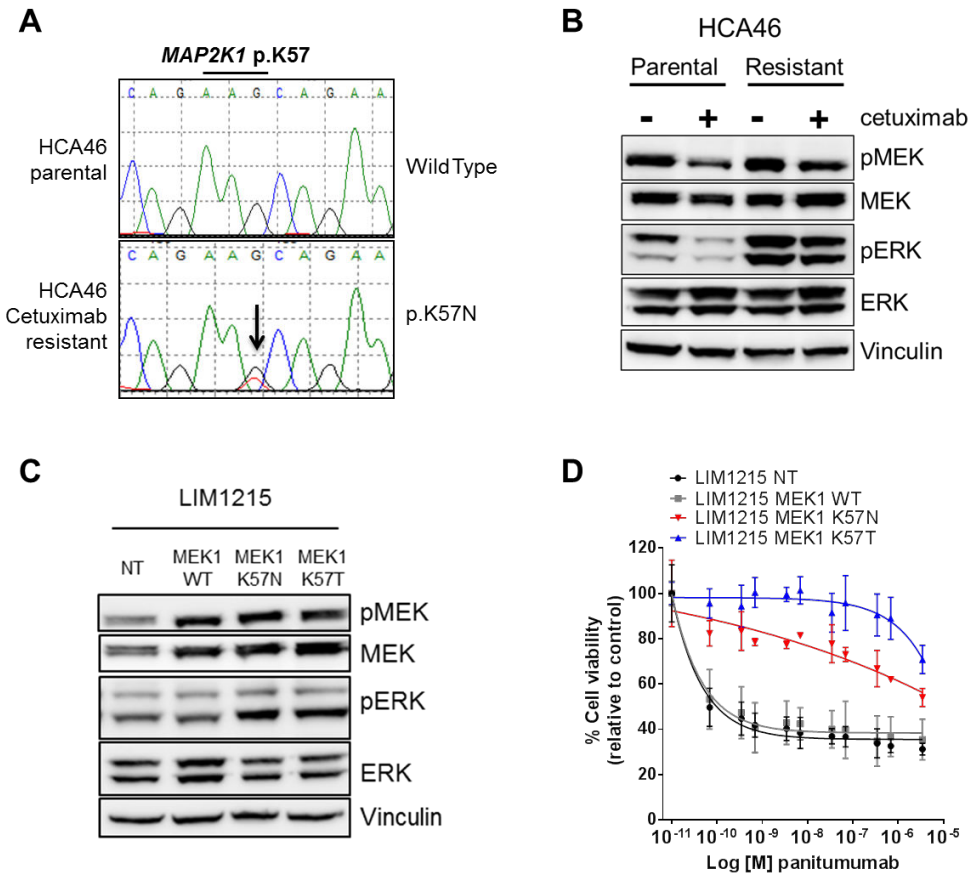

Supplementary Figure S1. MEK1 K57 mutations confer resistance to anti-EGFR antibodies in CRC preclinical models

Cetuximab-resistant cells, generated from the CRC cell line HCA46, harbor a MEK1 K57N mutation as shown in the electropherogram in panel A. HCA46 *RAS*-wildtype parental cell lines harbor wildtype MEK1. In panel B, parental HCA46 cells and cetuximab-resistant HCA46 clones (harboring MEK1 K57N mutation) were treated with or without cetuximab 50μg/ml for 24h and western blotting was performed with the indicated antibodies. Panel C shows a western blot of LIM1215 CRC cells exogenously expressing wildtype (WT), K57N, or K57T MEK1. NT indicates not transduced cells. In panel D exogenous expression of MEK1 K57T or MEK1 K57N in an independent

cetuximab-sensitive *RAS*-wildtype colorectal cancer cell line (LIM1215) confers resistance to panitumumab, relative to expression of wildtype MEK1. NT indicates not transduced cells.

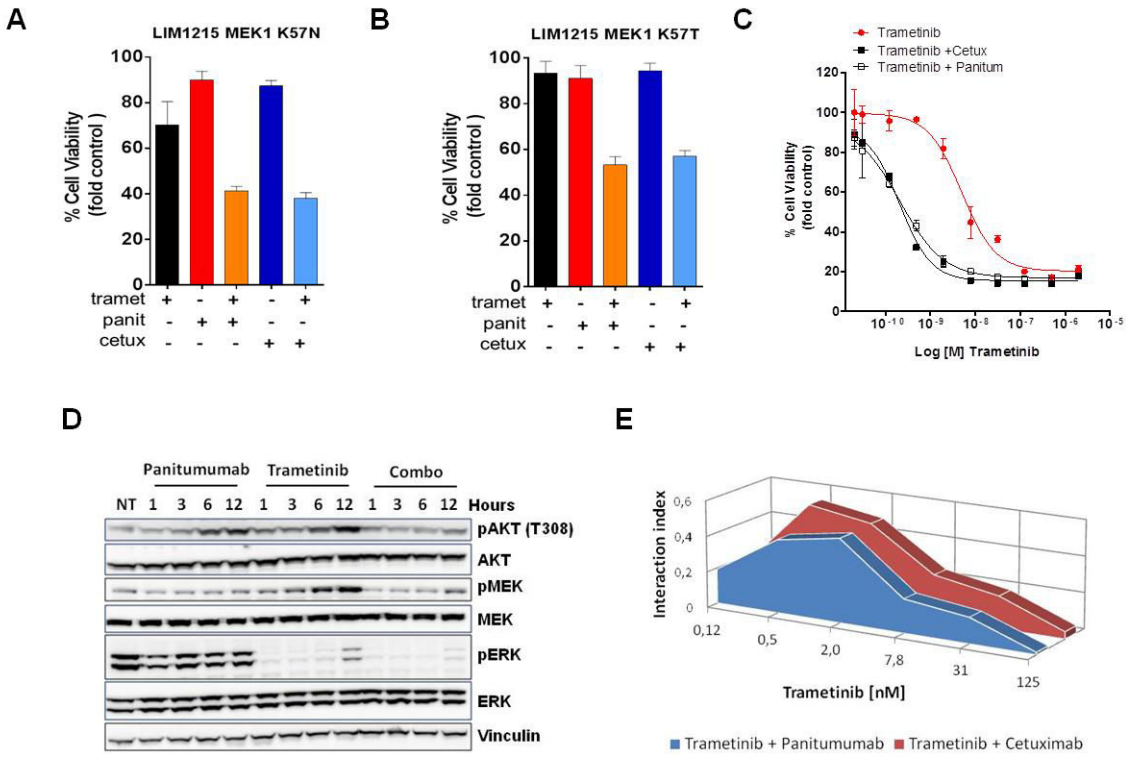

Supplementary Figure S2. Dual blockade of EGFR and MEK restores sensitivity to CRC cells expressing MEK1 K57N or K57T.

The combination of cetuximab (cetux) and trametinib (tramet) or panitumumab (panit) and trametinib (tramet) can restore sensitivity to LIM1215 CRC cells exogenously expressing MEK1 K57N (panel A) or K57T (panel B). In panel C anti-EGFR antibodies enhance the efficacy of trametinib on HCA46 cetuximab-resistant cells harboring a MEK1 K57N mutation. Cells were treated with increasing concentrations of trametinib and panitumumab (panitum) or cetuximab (cetux). Cell viability was assessed by measuring ATP content after 5 days of treatment. In Panel D, combinatorial treatment of panitumumab and trametinib is necessary to achieve a prolonged downregulation of both PI3K and MAPK pathways in HCA46 cetuximab resistant cells. Cell lines were treated with trametinib 50nM, panitumumab 50µg/ml, or the combination of both at the indicated time points, after which whole-cell extracts were subjected to western blot

analysis and membranes were probed with indicated antibodies. Vinculin was included as a loading control. (E) Bliss interaction index between trametinib (MEKi) and anti-EGFR antibodies (cetuximab and panitumumab) in HCA46 cetuximab-resistant cells. Synergism, additivity, or antagonism is indicated by an Interaction Index >0, ≈0 or <0, respectively. The interaction index is greater than 0 across all trametinib concentrations tested, indicating that its combination with either cetuximab or panitumumab has synergistic effects.

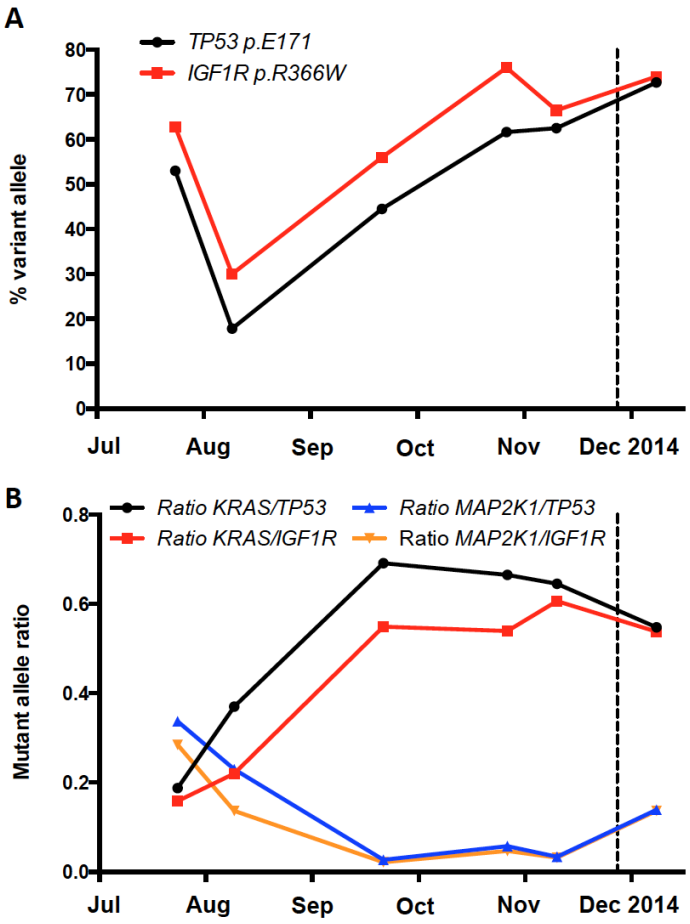

Supplementary Figure S3. Longitudinal analysis of founder mutations in patient plasma during panitumumab and trametinib treatment. Serial assessments of plasma circulating tumor DNA for the percent abundance of variant alleles for *TP53* p.E171* and *IGF1R* p.R366W are shown throughout treatment (panel A). In Panel B, the ratio of either *MAP2K1* p.K57T or *KRAS* p.Q61H to each founder mutation (*TP53* p.E171* or *IGF1R* p.R366W) is shown throughout treatment.

Supplementary Tables

1000 GENE PANEL															
AAK1	BLK	CDK15	CSNK2A2	EPHB3	FUS	IKZF1	LMTK2	MDS2	NF1	PEAK1	PRKACG	RPS6KA2	SRPK3	TIE1	WHSC1L1
AATK	BLM	CDK16	CTNNB1	EPHB4	FYN	IL2	LMTK3	MECOM	NF2	PER1	PRKAR1A	RPS6KA3	SRSF3	TIMP3	WHSC2
ABI1	BMI1	CDK17	CUBN	EPHB6	GAB1	IL21R	LPP	MEF2B	NFE2L2	PGF	PRKCA	RPS6KA4	SS18	TLK1	WIF1
ABL1	BMP2K	CDK18	CXCL1	EPS15	GABRA6	IL6ST	LRP1B	MELK	NFIB	PHF6	PRKCB	RPS6KA5	SS18L1	TLK2	WNK1
ABL2	BMPR1A	CDK19	CXCR7	ERBB2	GAK	IL7R	LRRK1	MEN1	NFKB1	PHKG1	PRKCD	RPS6KA6	SSX1	TLX1	WNK2
ACSL3	BMPR1B	CDK2	CYLD	ERBB3	GAS7	ILK	LRRK2	MERTK	NFKB2	PHKG2	PRKCE	RPS6KB1	SSX2	TLX3	WNK3
ACSL6	BMPR2	CDK20	DAPK1	ERBB4	GATA1	INPP4A	LTK	MET	NFKBIA	PHOX2B	PRKCG	RPS6KB2	SSX4	TMPRSS2	WNK4
ACTR2	BMX	CDK3	DAPK2	ERC1	GATA2	INSR	LYL1	MINK1	NFKBIE	PI4K2A	PRKCH	RPS6KC1	STIL	TNFAIP3	WRN
ACVR1	BRAF	CDK4	DAPK3	ERCC2	GATA3	INSRR	LYN	MITF	NIM1	PI4K2B	PRKCI	RPS6KL1	STK10	TNFRSF14	WT1
ACVR1B	BRCA1	CDK5	DAXX	ERCC3	GCK	IP6K1	MAF	MKL1	NIN	PI4KA	PRKCQ	RUNDC2A	STK11	TNFRSF17	XPA
ACVR1C	BRCA2	CDK6	DBN1	ERCC4	GMPS	IP6K2	MAFB	MKNK1	NKX2-1	PI4KB	PRKCZ	RUNX1	STK16	TNIK	XPC
ACVR2A	BRD2	CDK7	DCLK1	ERCC5	GNA11	IP6K3	MAK	MKNK2	NLK	PICALM	PRKD1	RUNX1T1	STK17A	TNK1	YES1
ACVR2B	BRD3	CDK8	DCLK2	ERG	GNAQ	IPMK	MALAT1	MLF1	NONO	PIK3C2A	PRKD2	RYK	STK17B	TNK2	YSK4
ACVRL1	BRD4	CDK9	DCLK3	ERN1	GNAS	IPPK	MALT1	MLH1	NOS3	PIK3C2B	PRKD3	SBDS	STK19	TNNI3K	ZAK
ADAMTSL3	BRDT	CDKL1	DDB2	ERN2	GOLGA5	IRAK1	MAML2	MLKL	NOTCH1	PIK3C2G	PRKDC	SBK1	STK24	TOP1	ZAP70
ADCK1	BRIP1	CDKL2	DDIT3	ESR1	GOPC	IRAK2	MAP2K1	MLL	NOTCH2	PIK3C3	PRKG1	SBK2	STK25	TOP2A	ZBTB16
ADCK3	BRSK1	CDKL3	DDR1	ESR2	GPC3	IRAK3	MAP2K2	MLL2	NOTCH3	PIK3CA	PRKG2	SCML2	STK3	TP53	ZMYM2
ADCK4	BRSK2	CDKL4	DDR2	ETV1	GPHN	IRAK4	MAP2K3	MLL3	NPM1	PIK3CB	PRKX	SCYL1	STK31	TP53RK	ZMYND8
ADCK5	BTG1	CDKL5	DDX10	ETV4	GRB2	IRF4	MAP2K4	MLLT1	NPR1	PIK3CD	PRKY	SCYL2	STK32A	TP73	ZNF331
ADRBK1	BTK	CDKN2A	DDX5	ETV5	GRK1	IRS2	MAP2K5	MLLT10	NPR2	PIK3CG	PRPF4B	SCYL3	STK32B	TPM3	ZNF384
ADRBK2	BUB1	CDKN2B	DDX6	ETV6	GRK4	IRS4	MAP2K6	MLLT11	NR4A3	PIK3R1	PRRX1	SDHAF2	STK32C	TPM4	ZNF521
AFF1	BUB1B	CDKN2C	DEK	EWSR1	GRK5	ITGA9	MAP2K7	MLLT3	NRAS	PIK3R2	PSIP1	SDHB	STK33	TPR	
AFF3	C15ORF55	CDX2	DGKA	EXT1	GRK6	ITGAV	MAP3K1	MLLT4	NRBP1	PIK3R3	PSKH1	SDHC	STK35	TRIB1	
AFF4	C9orf96	CEBPA	DGKB	EXT2	GRK7	ITGB3	MAP3K10	MLLT6	NRBP2	PIK3R4	PSKH2	SDHD	STK36	TRIB2	
AGK	CADM1	CERK	DGKD	EZH2	GSG2	ITGB5	MAP3K11	MN1	NRK	PIK3R5	PTCH1	SEPT5	STK38	TRIB3	
AKAP9	CAMK1	CHCHD7	DGKE	FAM123A	GSK3A	ITK	MAP3K12	MNX1	NRP1	PIK3R6	PTEN	SEPT6	STK38L	TRIM24	
AKT1	CAMK1D	CHD1	DGKG	FAM123B	GSK3B	ITPK1	MAP3K13	MOS	NSD1	PIKFYVE	PTK2	SEPT9	STK39	TRIM27	
AKT2	CAMK1G	CHD1L	DGKH	FAM123C	GUCY1A2	ITPKA	MAP3K14	MPL	NTRK1	PIM1	PTK2B	SERPINE1	STK4	TRIM28	
AKT3	CAMK2A	CHD3	DGKI	FANCA	GUCY2C	ITPKB	MAP3K15	MSH2	NTRK2	PIM2	PTK6	SET	STK40	TRIM33	
ALDH2	CAMK2B	CHD5	DGKQ	FANCC	GUCY2D	ITPKC	MAP3K2	MSH6	NTRK3	PIM3	PTK7	SETD2	STRADA	TRIO	
ALK	CAMK2D	CHEK1	DGKZ	FANCD2	GUCY2F	JAK1	MAP3K3	MSI2	NUAK1	PINK1	PTPN11	SETDB1	STRADB	TRIP11	
ALPK1	CAMK2G	CHEK2	DHFR	FANCE	HAUS3	JAK2	MAP3K4	MSN	NUAK2	PIP4K2A	PTPN2	SFPQ	STYK1	TRPM6	
ALPK2	CAMK4	CHIC2	DICER1	FANCF	HCK	JAK3	MAP3K5	MST1R	NUMA1	PIP4K2B	PXK	SGK1	SUFU	TRPM7	
ALPK3	CAMKK1	CHN1	DMPK	FANCG	HDAC9	JAZF1	MAP3K6	MST4	NUP214	PIP4K2C	RABEP1	SGK196	SUZ12	TRRAP	
AMHR2	CAMKK2	CHUK	DNMT3A	FAS	HERPUD1	JUN	MAP3K7	MTCP1	NUP98	PIP5K1A	RAC1	SGK2	SYK	TSC1	
ANGPT2	CAMKV	CIC	DSTYK	FASTK	HGF	JUNB	MAP3K8	MTOR	OBSCN	PIP5K1B	RAD51B	SGK223	TAF1	TSC2	
ANKK1	CANT1	CIITA	DUX4	FAT3	HIF1A	KALRN	MAP3K9	MUC1	OLIG2	PIP5K1C	RAF1	SGK3	TAF15	TSHR	
APC	CARD11	CIT	DYRK1A	FBXW7	HIP1	KAT6A	MAP4K1	MUSK	OMD	PIP5KL1	RAGE	SGK494	TAF1L	TSSK1B	
AR	CARS	CLK1	DYRK1B	FCGR2B	HIPK1	KAT6B	MAP4K2	MUTYH	OXSR1	PIPSL	RALGDS	SH3GL1	TAL1	TSSK2	
ARAF	CASC5	CLK2	DYRK2	FCRL4	HIPK2	KDM5A	MAP4K3	MYB	P2RY8	PKDCC	RANBP17	SIK1	TAL2	TSSK3	
ARHGAP26	CASK	CLK3	DYRK3	FER	HIPK3	KDM5C	MAP4K4	MYC	PAFAH1B2	PKHD1	RAP1GDS1	SIK2	TAOK1	TSSK4	
ARHGEF12	CBFA2T3	CLK4	DYRK4	FES	HIPK4	KDM6A	MAP4K5	MYCL1	PAK1	PKLR	RARA	SIK3	TAOK2	TSSK6	
ARID1A	CBFB	CLP1	EBF1	FEV	HIST1H4I	KDM6B	MAPK1	MYCN	PAK2	PKMYT1	RB1	SIX4	TAOK3	TTBK1	
ARID5B	CBL	CLTC	EDNRB	FGF2	HLF	KDR	MAPK10	MYD88	PAK3	PKN1	RBM15	SLC45A3	TBCK	TTBK2	
ARNT	CBLB	CLTCL1	EEF2K	FGFR1	HMGA1	KDSR	MAPK11	MYH1	PAK4	PKN2	RECQL4	SLK	TBK1	TTK	
ASPSCR1	CBLC	CNBP	EFNA1	FGFR1OP	HMGA2	KIAA1468	MAPK12	MYH11	PAK6	PKN3	REL	SMAD2	TBX22	TTL	
ASXL1	CCDC6	CNKSR2	EGFR	FGFR2	HMGN2P46	KIAA1549	MAPK13	MYH9	PAK7	PLAG1	RET	SMAD4	TCEA1	TTN	
ATF1	CCNB1IP1	CNTRL	EHMT1	FGFR3	HNF1A	KIAA1804	MAPK14	MYLK	PALB2	PLCG1	RHEB	SMARCA4	TCF12	TXK	
ATIC	CCND1	COL1A1	EIF2AK1	FGFR4	HNRNPA2B1	KIT	MAPK15	MYLK2	PASK	PLCG2	RHOH	SMARCB1	TCF3	TYK2	
ATM	CCND2	COX6C	EIF2AK2	FGR	HOOK3	KLF6	MAPK3	MYLK3	PATZ1	PLK1	RIOK1	SMG1	TCL1A	TYRO3	
ATP8B1	CCND3	CREB1	EIF2AK3	FH	HOXA11	KLHL4	MAPK4	MYLK4	PAX3	PLK2	RIOK2	SMO	TCL6	UHMK1	
ATR	CCNE1	CREB3L1	EIF2AK4	FHIT	HOXA13	KLK2	MAPK6	MYO3A	PAX5	PLK3	RIOK3	SMYD4	TEC	ULK1	
ATRX	CD274	CREB3L2	EIF4A2	FIP1L1	HOXA9	KRAS	MAPK7	MYO3B	PAX7	PLK4	RIPK1	SNRK	TEK	ULK2	
AURKA	CD74	CREBBP	ELF4	FKBP8	HOXC11	KSR1	MAPK8	NACA	PAX8	PMEL	RIPK2	SNX4	TERT	ULK3	
AURKB	CD79A	CRK	ELK4	FLCN	HOXC13	KSR2	MAPK9	NBN	PBK	PML	RIPK3	SOCS1	TESK1	ULK4	
AURKC	CD79B	CRLF2	ELL	FLI1	HOXD11	KTN1	MAPKAPK2	NCKIPSD	PBRM1	PMS1	RIPK4	SOX2	TESK2	USP28	
AXIN1	CDC42BPA	CRP	ELN	FLNB	HOXD13	L3MBTL2	MAPKAPK3	NCOA1	PBX1	PMS2	RMI2	SP1	TET1	USP6	
AXL	CDC42BPB	CRTC1	EML4	FLT1	HRAS	L3MBTL3	MAPKAPK5	NCOA2	PCM1	PNCK	RNASEL	SPECC1	TET2	VCAM1	
BAP1	CDC42BPG	CRTC3	EP300	FLT3	HSP90AA1	LASP1	MARK1	NCOA4	PCSK7	POU2AF1	RNF213	SPEG	TEX14	VEGFA	
BCKDK	CDC6	CSF1R	EPHA1	FLT4	HSP90AB1	LATS1	MARK2	NEK1	PDCD1LG2	POU5F1	RNF220	SPHK1	TFDP1	VEGFB	
BCL10	CDC7	CSK	EPHA10	FNBP1	HSPB8	LATS2	MARK3	NEK10	PDE4DIP	PPARG	ROBO1	SPHK2	TFE3	VEGFC	
BCL11A	CDC73	CSMD3	EPHA2	FOXL2	HUNK	LCK	MARK4	NEK11	PDGFB	PPP2R1A	ROBO2	SPOP	TFEB	VHL	
BCL11B	CDH1	CSNK1A1	EPHA3	FOXO1	ICAM1	LCP1	MAST1	NEK2	PDGFRA	PRCC	ROCK1	SPP1	TFG	VPREB1	
BCL2	CDH11	CSNK1A1L	EPHA4	FOXO3	ICK	LEF1	MAST2	NEK3	PDGFRB	PRDM1	ROCK2	SPTAN1	TFPT	VRK1	
BCL3	CDK1	CSNK1D	EPHA5	FOXO4	IDH1	LHFP	MAST3	NEK4	PDIK1L	PRDM16	ROR1	SRC	TFRC	VRK2	
BCL6	CDK10	CSNK1E	EPHA6	FOXP1	IDH2	LIFR	MAST4	NEK5	PDK1	PRF1	ROR2	SRGAP3	TGFBR1	VRK3	
BCL7A	CDK11B	CSNK1G1	EPHA7	FRK	IGF1R	LIMK1	MASTL	NEK6	PDK2	PRKAA1	ROS1	SRM	TGFBR2	WAS	
BCL9	CDK12	CSNK1G2	EPHA8	FRS2	IGF2R	LIMK2	MATK	NEK7	PDK3	PRKAA2	RPL22	SRMS	TGFBR3	WEE1	
BCR	CDK13	CSNK1G3	EPHB1	FSCB	IKBKB	LMO1	MDM2	NEK8	PDK4	PRKACA	RPN1	SRPK1	THRAP3	WEE2	
BIRC3	CDK14	CSNK2A1	EPHB2	FSTL3	IKBKE	LMO2	MDM4	NEK9	PDPK1	PRKACB	RPS6KA1	SRPK2	TIAM1	WHSC1	

Supplementary Table S1. 1000 gene sequencing panel. The primary tumor and segment 8 liver metastasis were analyzed using a sequencing panel providing full exome coverage of the genes listed in the table.

40 GENE PANEL	
AKT1	IDH1
ALK	IDH2
APC	KIT
BRAF	KRAS
CDH1	MAP2K1
CDKN2A	MET
CTNNB1	NOTCH
DDR2	NRAS
EGFR	PDGFRA
ERBB2	PIK3CA
ESR1	PIK3R1
FBXW7	PTEN
FGFR1	RET
FGFR2	ROS1
FGFR3	SMAD4
FOXL2	SMO
GNA11	STK11
GNAQ	TERTprmt
GNAS	TP53
HRAS	VHL

Supplementary Table S2. 40 gene targeted sequencing panel. Patient's tumor tissue specimen were analyzed using a clinical next generation sequencing assay covering these 40 cancer-related genes.

LESION	TARGET	MUT READS	WT READS	FRACTIONAL ABUNDANCE (%)	DETECTED BY ddPCR
1.) Left colectomy	***TP53* p.E171***	124	363	34.2	+
	***MAP2K1* (MEK1) p.K57T**	0	93	0	-
	***KRAS* p.Q61H**	0	251	0	-
2.) Low anterior resection	***TP53* p.E171***	5	93	5.4	+
	***MAP2K1* (MEK1) p.K57T**	0	89	0	-
	***KRAS* p.Q61H**	0	96	0	-
3.) Partial hepatectomy	***TP53* p.E171***	167	322	51.9	+
	***MAP2K1* (MEK1) p.K57T**	0	416	0	-
	***KRAS* p.Q61H**	0	817	0	-
4.) post-progression biposy (segment 8 liver lesion)	***TP53* p.E171***	299	474	63.1	+
	***MAP2K1* (MEK1) p.K57T**	35	309	11	+
	***KRAS* p.Q61H**	0	256	0	-
5.) progressing segment 5 liver lesion	***TP53* p.E171***	151	387	39.0	+
	***MAP2K1* (MEK1) p.K57T**	0	186	0	-
	***KRAS* p.Q61H**	92	302	30	+

Supplementary Table S3. Summary of targeted sequencing and ddPCR data on tissue specimens. Each tissue specimen obtained was analyzed by NGS (40 gene panel) and droplet digital PCR (ddPCR). The number of mutant (MUT) or wildtype (WT) sequencing reads and the relative fractional abundance for each variant shown are indicated.

COSMIC occurrence	gene	variant effect	variant	WT reads	MUT reads	Fractional abundance (%)
29	*TP53*	stopgain	p.E171*	219	249	53.0
207	*KRAS*	nonsynonymous	p.Q61H	199	15	7.0
8	*MAP2K1*	nonsynonymous	p.K57T	166	27	14.0
1	*NBN*	nonsynonymous	p.T268M	122	235	65.8
0	*IGF1R*	nonsynonymous	p.R366W	15	33	68.8
0	*FGFR4*	stopgain	p.R416*	71	46	39.3
0	*KDR*	nonsynonymous	p.T761M	183	33	15.2
0	*CHEK2*	nonsynonymous	p.P552S	222	10	4.3

Supplementary Table S4. Next generation sequencing data from plasma ctDNA. The table shows the mutations found in the patient's plasma ctDNA (before initiation of panitumumab and trametinib) compared to genomic DNA isolated from peripheral blood mononuclear cells (PBMC) using the IRCC-TARGET next generation sequencing panel. To uncover somatic mutations, we compared germline (PBMC) and ctDNA samples, and identified basepair mismatches (Fisher's Test) with fractional abundance above 1%. Mutations were then called only when supported by a 5% statistical significance and their occurrence was checked in the COSMIC database. Mutations were annotated by a custom script printing (from left to right) gene name, the variant effect (synonymous, non-synonymous, stop-loss/gain), protein change (variant), number of wildtype (WT) or mutated (MUT) reads and the allelic frequencies (fractional abundance). Every somatic mutation was validated by visual examination using BAM files. Sequencing coverage depth was 229x for PBMC and 213x for plasma.

GE/ml plasma	Blood draw	TARGET	MUT EVENTS ddPCR	WT EVENTS ddPCR	FRACTIONAL ABUNDANCE (%) ddPCR	MUT READS (NGS)	WT READS (NGS)	FRACTIONAL ABUNDANCE (%) (NGS)
121747	**Jul 2014**	***TP53* p.E171***	217	193	53	219	249	53.0
		***IGF1R* p.R366W**	601	356	62.8	15	33	68.8
		***MAP2K1*p.K57T**	92	423	17.9	166	27	14.0
		***KRAS* p.Q61H**	32	290	9.9	199	15	7.0
55950	**Aug 2014**	***TP53*p.E171***	38	175	18	NA		
		***IGF1R* p.R366W**	89	204	30			
		***MAP2K1*p.K57T**	10	234	4.1			
		***KRAS* p.Q61H**	14	198	6.6			
66532	**Sep 2014**	***TP53* p.E171***	101	126	44	NA		
		***IGF1R* p.R366W**	73	58	56			
		***MAP2K1*p.K57T**	4	330	1.2			
		***KRAS* p.Q61H**	103	232	30.8			
187088	**Oct 2014**	***TP53* p.E171***	201	125	62	NA		
		***IGF1R* p.R366W**	1027	325	76			
		***MAP2K1*p.K57T**	32	870	3.6			
		***KRAS* p.Q61H**	243	350	41			
1462004	**Nov 2014**	***TP53* p.E171***	445	267	63	NA		
		***IGF1R* p.R366W**	537	271	66.5			
		***MAP2K1*p.K57T**	21	980	2,1			
		***KRAS* p.Q61H**	862	1277	40.3			
2725500	**Dec 2014**	***TP53* p.E171***	1991	748	73	63	34	64.9
		***IGF1R* p.R366W**	181	63	74	68	13	83.9
		***MAP2K1*p.K57T**	218	1940	10.1	19	146	11.5
		***KRAS* p.Q61H**	1539	2328	39.8	74	126	37.0

Supplementary Table S5. Summary of serial ctDNA analyses. Circulating tumor DNA (ctDNA) was isolated from serial blood draws collected before initiation of panitumumab and trametinib (Jul 2014), throughout treatment, and after discontinuation of therapy (Dec 2014). Each time point was analyzed by droplet digital PCR (ddPCR). The number of Genome Equivalents (GE), mutated (MUT) and wild type (WT) events and fractional abundance are listed. Plasma from week 0 and 19 were analyzed also with the IRCC-

TARGET panel(4). Mutated (MUT) and wild type (WT) reads and fractional abundance are listed. Sequencing coverage depth was 213x for week 0 and 140x for week 19.

	TP53 p.E171* (%)	*IGF1R* p.R366W (%)	*KRAS* p.Q61H (%)	*MAP2K1* p.K57T (%)	RATIO KRAS/TP53 (%)	RATIO KRAS/IGF1R (%)	RATIO MAP2K1/TP53 (%)	RATIO MAP2K1/IGF1R (%)
Jul	53,0	62,8	9,9	17,9	18,7	15,8	33,8	28,5
Aug	18,0	30,0	6,6	4,1	36,7	22,0	22,8	13,7
Sep	44,0	56,0	30,7	1,2	69,9	54,9	2,7	2,1
Oct	62,0	76,0	41,0	3,5	66,1	53,9	5,7	4,7
Nov	63,0	66,5	40,3	2,1	64,0	60,6	3,3	3,2
Dec	73,0	74,0	39,8	10,1	54,5	53,8	13,8	13,7

Supplementary Table S6. Ratio of resistance-associated genetic alterations and founder mutations in serial plasma ctDNA timepoints. Table lists mutational frequency and ratio (%) between founder (*TP53* p.E171* and *IGF1R* p.R366W) and resistance-associated genetic alterations (*KRAS* p.Q61H and *MAP2K1* p.K57T) assessed by ddPCR in serial plasma ctDNA timepoints.

REFERENCES

1. Li H, Durbin R. Fast and accurate long-read alignment with Burrows-Wheeler transform. Bioinformatics 2010;26(5):589-95.
2. Li H, Handsaker B, Wysoker A, Fennell T, Ruan J, Homer N, et al. The Sequence Alignment/Map format and SAMtools. Bioinformatics 2009;25(16):2078-9.
3. Ye K, Schulz MH, Long Q, Apweiler R, Ning Z. Pindel: a pattern growth approach to detect break points of large deletions and medium sized insertions from paired-end short reads. Bioinformatics 2009;25(21):2865-71.

4. Siravegna G, Mussolin B, Buscarino M, Corti G, Cassingena A, Crisafulli G, et al. Clonal evolution and resistance to EGFR blockade in the blood of colorectal cancer patients. Nature medicine 2015.